

# Solid-state synthesis of graphite carbon-coated $\text{Li}_4\text{Ti}_5\text{O}_{12}$ anode for lithium ion batteries

Ying Wang · Wei Zou · Xinyi Dai · Lidong Feng ·  
Haiquan Zhang · Aijun Zhou · Jingze Li

Received: 6 January 2014 / Revised: 13 February 2014 / Accepted: 1 March 2014  
© Springer-Verlag Berlin Heidelberg 2014

**Abstract** Graphites are widely used for their high electrical conductivity and good thermal and chemical stability. In this work, graphitic carbon-coated lithium titanium ( $\text{Li}_4\text{Ti}_5\text{O}_{12}/\text{GC}$ ) was successfully synthesized by a simple one-step solid-state reaction process with the assistance of sucrose without elevating sintering temperature. The lattice fringe of 0.208 nm clearly seen from the high-resolution transmission electron microscopy (HRTEM) images was assigned to graphite (010). The average grain size of the as-prepared  $\text{Li}_4\text{Ti}_5\text{O}_{12}/\text{GC}$  was about 100–200 nm, 1 order smaller than that of pure  $\text{Li}_4\text{Ti}_5\text{O}_{12}$  prepared similarly. The rate performance and cycle ability were significantly improved by the hybrid conducting network formed by graphitic carbon on the grains and amorphous carbon between them. The specific capacity retention rate was 66.7 % when discharged at a rate of 12C compared with the capacity obtained at 0.5C. After 300 cycles, the capacity retention was more than 90 % at a high rate of 15C.

**Keywords** Batteries ·  $\text{Li}_4\text{Ti}_5\text{O}_{12}$  · Solid-state reactions · Graphitic carbon · Anodes

## Introduction

Lithium ion batteries offering higher power and higher energy density have been powering most of the portable electronic devices [1]. Furthermore, the increasing crisis of traditional energy resources and serious concerns on global environment are making lithium ion batteries to enable electric vehicles

(EVs) and hybrid electric vehicles (HEVs) and be a complement to wind and solar energy [2, 3]. Compared with traditional carbon-related anodes and alloy anodes,  $\text{Li}_4\text{Ti}_5\text{O}_{12}$  exhibits excellent reversibility between spinel structure and rock-salt structure after numerous  $\text{Li}^+$  insertion and extraction processes, which contributes to excellent cycling stability [4]. Together with a high operating potential of 1.55 V vs.  $\text{Li}/\text{Li}^+$  avoiding the formation of lithium dendrites [5],  $\text{Li}_4\text{Ti}_5\text{O}_{12}$  is proposed as an ideal candidate anode for HEVs and stationary energy storage [6, 7]. Recently,  $\text{Li}_4\text{Ti}_5\text{O}_{12}$  was newly reported as a wonderful  $\text{Na}^+$  storage material [8]. But the poor rate performance of pristine  $\text{Li}_4\text{Ti}_5\text{O}_{12}$  caused by low electronic conductivity (less than  $10^{-13} \text{ S cm}^{-1}$  [9]) prevents it from practical use. Many efforts have been made to improve the electronic conductivity by cation doping (such as K, Al, V, Nb, etc. [10–13]), surface modification (such as polyacene [14], carbon [15–18] or N-doped carbon [19–21]), or composites ( $\text{Li}_4\text{Ti}_5\text{O}_{12}/\text{TiO}_2$  [22–24],  $\text{Li}_4\text{Ti}_5\text{O}_{12}/\text{Ag}$  [25],  $\text{Li}_4\text{Ti}_5\text{O}_{12}/\text{Li}_2\text{Ti}_3\text{O}_7$  [26], etc.). Methods to increase  $\text{Li}^+$  transport ability or shorten  $\text{Li}^+$  diffusion length [27–30] were also extensively studied. The carbon coating technique has attracted much attention due to its simplicity and feasibility, where a diversity of carbon sources (e.g., pitch [18], ionic liquid [21], etc.) and fabrication methods (sol-gel method [17], solid-state reaction [15, 16], etc.) were investigated. It should be noted that most of the carbon layers are in the amorphous state [31]. It is well known that the conductivity of graphite is much better than that of amorphous carbon [32]. Generally, the carbon materials can be graphitized until the critical temperature is over 1,800 °C with a longer treating period [33]. In this regard, it is understandable why the graphitized carbon layer is rarely applied to coat  $\text{Li}_4\text{Ti}_5\text{O}_{12}$ .

Herein, we proposed an economic and easy to be scaled up route to synthesize graphitized carbon-coated  $\text{Li}_4\text{Ti}_5\text{O}_{12}$  composite in a low temperature. Sucrose was used as a carbon source, which was mixed with lithium salt and titanium

Y. Wang · W. Zou · X. Dai · L. Feng · H. Zhang · A. Zhou ·  
J. Li (✉)

State Key Laboratory of Electronic Thin Films and Integrated  
Devices, School of Microelectronics and Solid-state Electronics,  
University of Electronic Science and Technology of China, No. 4,  
Section 2, North Jianshe Road, Chengdu 610054, Sichuan, China  
e-mail: lijingze@uestc.edu.cn

compound. Then, the mixture was directly sintered by a simple one-step solid-state reaction. The graphitized carbon coating layer can efficiently prevent  $\text{Li}_4\text{Ti}_5\text{O}_{12}$  nanoparticles from aggregation, leading to the feature size down to around 200 nm. The composite showed excellent rate performance even charging/discharging at a high current rate of 12C, which was attributed to the improved electronic conductivity as well as the reduced  $\text{Li}^+$  diffusion length.

## Experimental

$\text{TiO}_2$  (anatase, averaged particle diameter 150 nm),  $\text{Li}_2\text{CO}_3$ , and sucrose were chosen as the starting materials. Sucrose accounted for X (X=0, 10, 15, 20) percent of the total weight of  $\text{TiO}_2$  and  $\text{Li}_2\text{CO}_3$ . All the starting materials were mixed in a liquid medium of acetone and water by a planetary ball mill for 4 h. The ball feed ratio was 5:1. The as-prepared slurry was then dried at 80 °C and ground into fine powder for later use. Following that, the ternary precursor was treated at a rate of 3 °C/min from room temperature to 800 °C in a tube furnace filled with argon gas, holding the maximum temperature for 12 h and natural cooling afterwards. The as-synthesized samples were named as LTOCX (X=0, 10, 15, 20).

The morphology of the as-synthesized samples was characterized by a field emission scanning electron microscope (FE-SEM, Hitachi, S3400N) and a transmission electron microscope (TEM, JEOL, JEM-100CX). The phase analysis was carried out with X-ray diffraction (XRD, X'Pert PRO MPD) using  $\text{Cu K}\alpha$  radiation, and the data was collected with a  $2\theta$  scan ranging from 15° to 85° at a step size of 0.03°. Raman spectra were measured by a Renishaw inVia Reflex Raman Microscope at a laser power of 0.5 mW with the excitation wavelength of 514 nm.

Two-electrode lab cell was assembled in a glove box circulated with argon gas (99.999 %) for electrochemical measurement. To produce the working electrode, the active material and acetylene black and polyvinylidene fluoride (PVDF) were dispersed in *N*-methyl-2-pyrrolidone (NMP) solution with a carnelian mortar. The weight ratio of the above three solid species was set to be 80:10:10. The electrode fabrication was finished by spreading the ground mixture on a thin Cu foil with the doctor-blade method and drying at 110 °C in a vacuum drying oven for about 12 h before cell assembly. The counter electrode was of metallic Li foil. The electrolyte was  $\text{LiPF}_6$  (1 mol/l) dissolved in the mixture ethylene carbonate, diethyl carbonate, and dimethyl carbonate (1:1:1 in volume).

The galvanostatic discharge/charge measurements were conducted on a LAND series battery testing system (CT2001A, LAND Electronic Co.) at a potential range of 1.0–3.0 V with different discharge/charge rates varying from

0.2C to 20C. Cyclic voltammetry (CV) and electrochemical impedance spectroscopy (EIS) were performed on an electrochemical work station (Solartron Model 1287/1260A; Solartron Analytical). CV curves were recorded under a scan rate of 0.1 mV S<sup>-1</sup> at a potential range of 1.0–3.0 V. EIS was performed at a frequency range of 0.01 Hz–1.0 MHz with the voltage amplitude of 5 mV.

## Results and discussion

### Morphology characterization and phase identification

Figure 1 exhibits the XRD patterns of the as-synthesized LTOCX compounds. The pattern of LTOC0 demonstrates clear peaks located at 2θ degree of 18.3°, 35.6°, 43.2°, 57.2°, and 62.9°, which match the positions and relative intensities of the spinel  $\text{Li}_4\text{Ti}_5\text{O}_{12}$  diffraction peaks listed in PDF #49-0207 very well. No impurity phase was identified, suggesting LTOC0 consists of pristine  $\text{Li}_4\text{Ti}_5\text{O}_{12}$ . While the amount of carbon source is slightly increased, the XRD pattern does not show a noticeable change considering either the peak position or the intensity. When the weight ratio of sucrose is increased to 20 % (LTOC20), unexpected diffraction peaks of  $\text{Li}_2\text{TiO}_3$  and anatase  $\text{TiO}_2$  appear, suggesting the pyrolyzed carbon retarded the reaction. This phenomenon was frequently observed while the carbon weight ratio is over the critical point. All of the XRD curves do not show any signal of carbon, indicating that the total weight of the carbon material might be too low or the pyrolyzed carbon is amorphous.

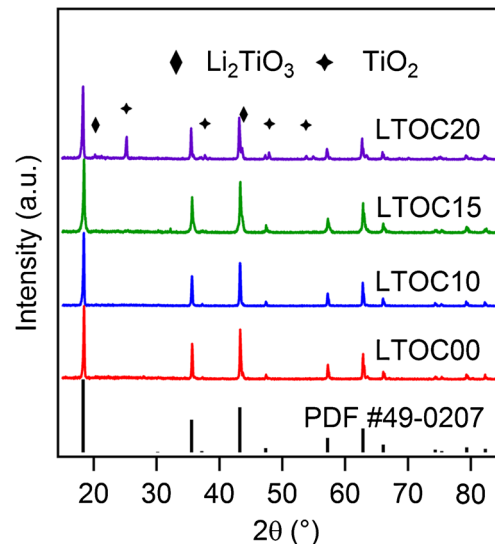
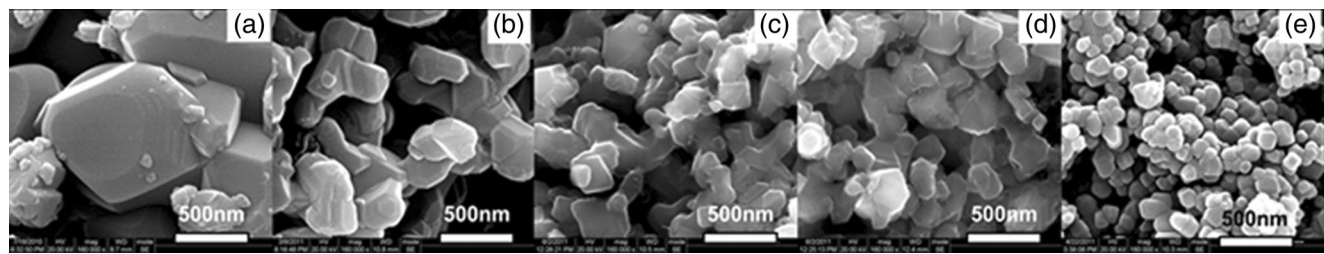


Fig. 1 XRD patterns of LTOCXs and PDF #49-0207



**Fig. 2** SEM images of LTOCXs and  $\text{TiO}_2$ : **a** LTOC00, **b** LTOC10, **c** LTOC15, **d** LTOC20, and **e**  $\text{TiO}_2$  used in the experiments

Figure 2 shows the corresponding SEM images of the as-synthesized LTOCX compounds. As a reference, the SEM image of the  $\text{TiO}_2$  reactant is also provided. The particle size of the pristine  $\text{Li}_4\text{Ti}_5\text{O}_{12}$  (LTOC0) is over 500 nm, and each particle is well crystallized, exposing very clear and flat facets. The introduction of 10 % weight of carbon source (LTOC10) can significantly reduce the particle size [34], in which the estimated average size is around 200 nm. The smaller particle will shorten  $\text{Li}^+$  diffusion distance and offer larger reaction area, which would provide benefit by reducing the electrochemical polarization and promoting the rate performance [35]. With the increased amount of the carbon source, the product becomes more uniform and its size can be further decreased slightly. The tendency is consistent with the published result, where the  $\text{TiO}_2$  precursor was coated with carbon layer prior to the solid-state reaction [16, 36]. However, it should be mentioned that the particle size of the sample with the highest carbon ratio (LTOC20) is larger than that of the  $\text{TiO}_2$  reactant, suggesting that the aggregation occurred in the process of thermal annealing. Even though the carbon source ratio was up to 20 % (LTOC20), it is still very difficult to identify if the pyrolyzed carbon is coated on  $\text{Li}_4\text{Ti}_5\text{O}_{12}$  nanoparticles by SEM imaging. TEM and high-resolution transmission electron microscopy (HRTEM) images of the composite LTOC15 are given in Fig. 3. Figure 3a exhibits a low magnification TEM image, where the particle size is around

200 nm. It is in accordance with SEM observation. The spider network is visible in the neighboring particle, which must be made of pyrolytic carbon. The enlarged TEM image exhibits that the carbon material is potted uniformly on the surface of well-crystallized  $\text{Li}_4\text{Ti}_5\text{O}_{12}$  grains. The HRTEM image illustrates that there are clear strip lines for each dot, and the spacing of the lattice fringe is 0.208 nm, which can be assigned to graphite (010). The maximum height of the dot is around 4 nm, and the minimum height is around 1 nm. More importantly, the neighboring dots are overlapped. That is to say, a serrated graphitized carbon layer is successfully coated on  $\text{Li}_4\text{Ti}_5\text{O}_{12}$ .

In order to make sure that graphitized carbon was formed in the macroscopic area, Raman spectrum was collected as shown in Fig. 4. The peaks located at 1,340 and 1,595  $\text{cm}^{-1}$  can be assigned to D and G bands, respectively. It is common knowledge that D band represents the vibration mode from amorphous carbon and G band originates from graphitized carbon [37]. The two peaks have comparable intensity, suggesting that the two types of carbon may have similar weight ratio. A large amount of defects on the surface of graphite grains also contributes to the low peak intensity ratio of the G band to D band [38]. According to HRTEM result, it can be easy to know that the particle is coated with graphitized carbon, and the neighboring particles were connected with amorphous carbon network. The nature of the starting material

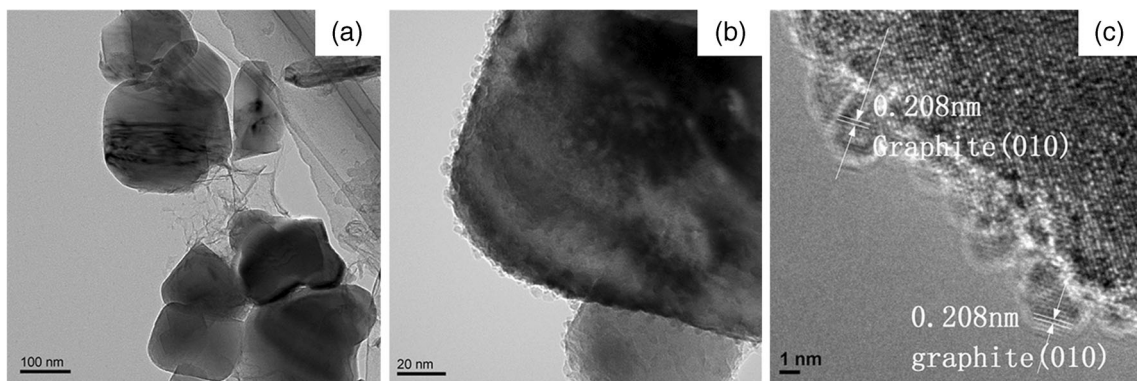


**Fig. 3** TEM and HRTEM images of sample LTOC15: **a** at low resolution, **b** high magnification of random grains, and **c** HRTEM of surface area of a random grain

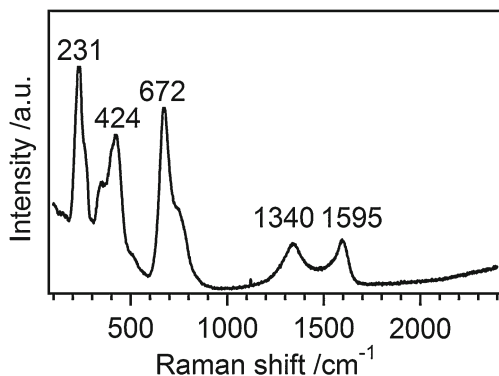


**Fig. 4** Raman spectrum of LTOC15

(sucrose) is suggested to be the shifts of the Raman peaks of carbon [39].

This result was different from that discussed in former works in which amorphous carbon was detected [24, 40]. The cooperation of relatively higher synthesis temperature and longer annealing time was suggested to be one of the reasons of graphitization. Atmosphere was another factor that affects the graphitization. The carbon layer tended to be amorphous if synthesized in  $\text{NH}_3$  atmosphere reported in our previous work [20].

#### Electrochemical performance

The typical charge/discharge profiles of LTOC15 at different current rates are shown in Fig. 5. The average initial specific capacity was  $183 \text{ mAh g}^{-1}$  when charged-discharged at a rate of  $0.5\text{C}$ , which is slightly higher than the theoretical value. The possible reason is that graphitic carbon exhibits electrochemical double layer capacitance effect above  $1.0 \text{ V}$  [41].

Due to the good conductivity of graphitic carbon coating outside the particles, the batteries prepared with sample LTOC15 show the best rate performance among all the samples. As shown in Fig. 6, high capacity retentions as  $154$ ,  $136$ ,

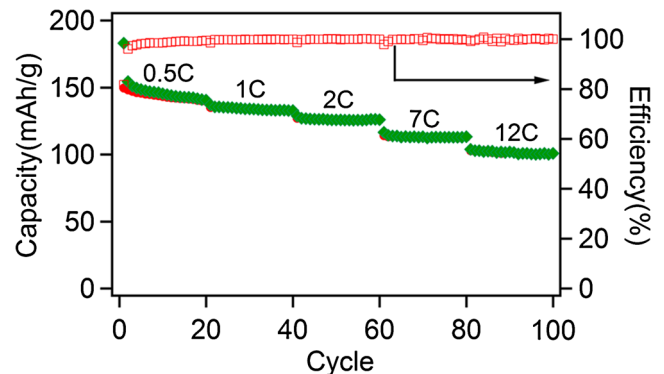


**Fig. 6** The rate performance of sample LTOC15 tested from 1 to 3 V

$127$ ,  $114$ , and  $102 \text{ mAh g}^{-1}$  were obtained even after being charged-discharged at  $0.5\text{C}$ ,  $1\text{C}$ ,  $2\text{C}$ ,  $7\text{C}$ , and  $12\text{C}$  for  $100$  cycles. Al foil was used as the current collector for comparison. The capacities are  $155$ ,  $133$ ,  $116$ ,  $88$ , and  $67 \text{ mAh g}^{-1}$ , respectively, which are much lower than those of the batteries with Cu foil as the current collector. The tendency agrees with the result reported by Hu [42]. The coulombic efficiency is over  $96\%$  after the second cycle and almost  $100\%$  afterwards. After  $300$  cycles, the capacity retention at a high level of more than  $90\%$  was achieved with a high discharge-charge rate of  $7\text{C}$  and  $15\text{C}$ , respectively (shown in Fig. 7). To compare the rate performance of all the samples, the normalization of the capacity variations based on the capacity at  $0.5\text{C}$  is exhibited in Fig. 8. Sample LTOC15 performed much better than that of sample LTOC0, but slightly better than that of sample LTOC20. It suggests that for sample LTOC15, a thin graphitic carbon layer on the grains and the pyrolyzed carbon among them have formed a nearly complete conducting network and improved the electron conductivity significantly. The smaller grain size and less agglomeration also contribute to the improvement. The results agree with TEM and Raman spectra well. The graphitic layer on the grains of sample LTOC20 is a

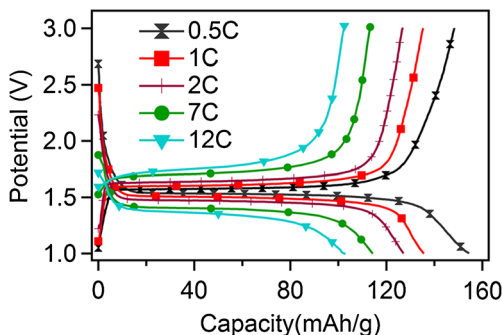


**Fig. 5** The charge-discharge data of sample LTOC15 tested from 1 to 3 V at different rates

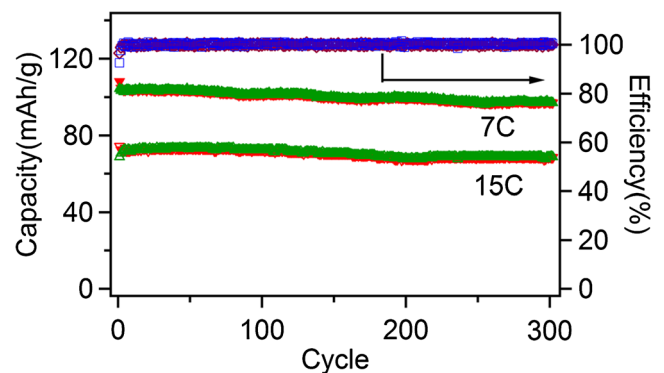


**Fig. 7** The cycle performance of sample LTOC15 tested from 1 to 3 V at the discharge-charge rates of  $7\text{C}$  and  $15\text{C}$

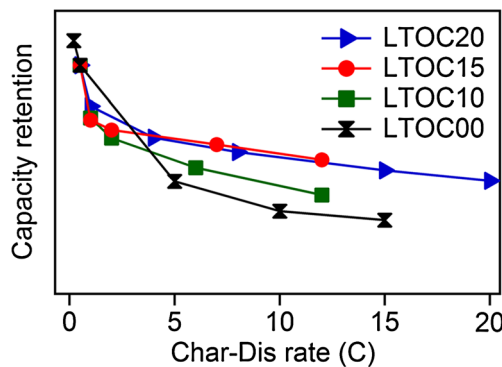


**Fig. 8** The capacity retention rates of the samples prepared with different percentages of sucrose

little thicker, which prevents  $\text{Li}^+$  from fast transport just like the case discussed in our previous work [20], that is why there is no further obvious improvement for sample LTOC20.

The irreversible capacity decline in the first cycle is presented in Table 1. The increased phase impurity in the samples is suggested to be the main reason of the capacity decline in the first cycle with the increasing weight ratio of sucrose involved [43].

To further demonstrate the effect of the graphitic carbon layer on the active materials. The first three cycles of CV measurement of samples LTOC0 and LTOC15 are shown in Fig. 9. Checking the figure, one dominant couple of redox peaks is observed while scanning at a rate of  $0.1 \text{ mV S}^{-1}$ . For pure  $\text{Li}_4\text{Ti}_5\text{O}_{12}$ , the cathodic peak and the anodic peak are located at 1.40 and 1.78 V, respectively, while for LTOC15, the two peaks are located at 1.45 and 1.66 V, which demonstrates that the graphitic carbon layer improves the electronic conductivity of the active materials. The coincidence of one to three cycles of the CV curves indicated the stability and reversibility of the discharge and charge process for pure and carbon-coated samples. This further indicates that there is no side effect when introducing sucrose (pyrolyzed carbon) in the material sintering process.

The AC impedance spectra were measured to further understand the conductivity of the graphite-coated  $\text{Li}_4\text{Ti}_5\text{O}_{12}$  material. The data are given in Fig. 10. The equivalent circuit is shown as an inset.  $R_{ct}$  of LTOC15, the equivalent resistance of the impedance caused by the electrochemical reaction

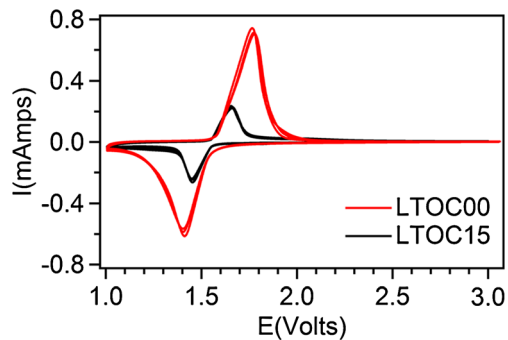


**Fig. 9** CV dates of samples LTOC0 and LTOC15 tested from 1 to 3 V at a scan rate of  $0.1 \text{ mV S}^{-1}$

activity at the interface between active material and electrolyte, is fitted to be  $86\Omega$ , which is much smaller than that of pure  $\text{Li}_4\text{Ti}_5\text{O}_{12}$  ( $170\Omega$ ). The result is comparable or better than the results mentioned in the literature [24, 44–46].

## Conclusions

Graphitic carbon-coated  $\text{Li}_4\text{Ti}_5\text{O}_{12}$  of high rate performance and good cycle stability was successfully achieved with the assistance of sucrose, which is cheap, environmentally friendly, and abundant in nature by a simple, short-time consumption, one-step solid-state reaction process. In this work, XRD, SEM, and TEM were carried out to study the physical characteristics. At both the aids of sucrose film coating on the grains of  $\text{Li}_2\text{CO}_3$  and  $\text{TiO}_2$ , the average grain size of the as-prepared graphite carbon-coated  $\text{Li}_4\text{Ti}_5\text{O}_{12}$  was tested to be around 100–200 nm, 1 order smaller than pristine  $\text{Li}_4\text{Ti}_5\text{O}_{12}$  prepared similarly. A good conducting network formed by graphitic carbon and pyrolyzed carbon can be seen from TEM photos. The less agglomeration and reduced grain size made the lithium ion diffusion much easier. As a result, the

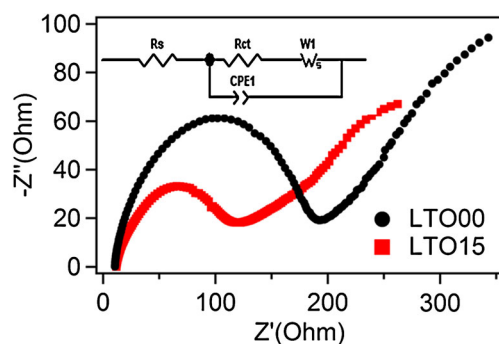


**Fig. 10** The AC impedance spectra of LTOC0 and LTOC15 measured at a stable voltage of 1.55 V in the frequency range of 0.01 Hz–1 MHz and the equivalent circuit used in data fitting

**Table 1** The capacity retention of the batteries fabricated by the samples in the initial cycles

Sample name	LTOC0	LTOC10	LTOC15	LTOC20
Initial capacity retention (%)	92	85	84	81

rate performance and cycle ability of graphitic carbon-coated  $\text{Li}_4\text{Ti}_5\text{O}_{12}$  were significantly improved. The specific capacity retained 66.7 % even at a rate of 12C compared with the capacity achieved when discharged at 0.5C. After the 300th cycle, the specific capacity retention was more than 90 % at a high rate of 15C. The work in this article is expected to be used in the mass production.

**Acknowledgments** This work was supported by NSFC (grant nos. 21073029, 11234013, and 51211140045), RFDP (no. 20100185110019), Program for New Century Excellent Talents in University (no. NCET-10-0296), and Fundamental Research Funds for the Central Universities (no. ZYGX2012Z003, 103.1.2 E022050205). The authors thank Miss Ming Liu, working at the Analytical and Testing Center of Sichuan University, China, for her help in TEM characterization.

## References

- Kang K, Meng YS, Bréger J, Grey CP, Ceder G (2006) Electrodes with high power and high capacity for rechargeable lithium batteries. *Science* 311(5763):977–980
- Sun YK, Myung ST, Park BC, Prakash J, Belharouak I, Amine K (2009) High-energy cathode material for long-life and safe lithium batteries. *Nat Mater* 8(4):320–324
- Kang B, Ceder G (2009) Battery materials for ultrafast charging and discharging. *Nature* 458(7235):190–193
- Lu X, Zhao L, He X, Xiao R, Gu L, Hu YS, Li H, Wang Z, Duan X, Chen L (2012) Lithium storage in  $\text{Li}_4\text{Ti}_5\text{O}_{12}$  spinel: the full static picture from electron microscopy. *Adv Mater* 24(24):3233–3238
- Ohzuku T, Ueda A, Yamamoto N (1995) Zero-strain insertion material of  $\text{Li}(\text{Li}_{1/3}\text{Ti}_{5/3})\text{O}_4$  for rechargeable lithium cells. *J Electrochem Soc* 142(5):1431–1435
- Guerfi A, Sevigny S, Lagace M, Hovington P, Kinoshita K, Zaghib K (2003) Nano-particle  $\text{Li}_4\text{Ti}_5\text{O}_{12}$  spinel as electrode for electrochemical generators. *J Power Sources* 119:88–94
- Zaghib K, Simoneau M, Armand M, Gauthier M (1999) Electrochemical study of  $\text{Li}_4\text{Ti}_5\text{O}_{12}$  as negative electrode for Li-ion polymer rechargeable batteries. *J Power Sources* 81:300–305
- Wang Y, Yu X, Xu S, Bai J, Xiao R, Hu YS, Li H, Yang XQ, Chen LQ, Huang XJ (2013) A zero-strain layered metal oxide as the negative electrode for long-life sodium-ion batteries. *Nature communications* 4: doi:10.1038/ncomms3365
- Chen C, Vaughney J, Jansen A, Dees D, Kahaian A, Goacher T, Thackeray M (2001) Studies of Mg-substituted  $\text{Li}_{4-x}\text{Mg}_x\text{Ti}_5\text{O}_{12}$  spinel electrodes ( $0 \leq x \leq 1$ ) for lithium batteries. *J Electrochem Soc* 148:A102–A104
- Li X, Qu MZ, Yu ZL (2010) Structural and electrochemical characteristics of  $\text{Li}_{4-x}\text{K}_x\text{Ti}_5\text{O}_{12}$  as anode material for lithium-ion batteries. *Chin J Inorg Chem* 26(2):233–239
- Zhao H, Li Y, Zhu Z, Lin J, Tian Z, Wang R (2008) Structural and electrochemical characteristics of  $\text{Li}_{4-x}\text{Al}_x\text{Ti}_5\text{O}_{12}$  as anode material for lithium-ion batteries. *Electrochim Acta* 53(24):7079–7083
- Yi TF, Shu J, Zhu YR, Zhu XD, Yue CB, Zhou AN, Zhu RS (2009) High-performance  $\text{Li}_4\text{Ti}_{5-x}\text{V}_x\text{O}_{12}$  ( $0 \leq x \leq 0.3$ ) as an anode material for secondary lithium-ion battery. *Electrochim Acta* 54(28):7464–7470
- Tian B, Xiang H, Zhang L, Wang H (2012) Effect of Nb-doping on electrochemical stability of  $\text{Li}_4\text{Ti}_5\text{O}_{12}$  discharged to 0 V. *J Solid State Electrochem* 16(1):205–211
- Yu H, Zhang X, Jalbout AF, Yan X, Pan X, Xie H, Wang R (2008) High-rate characteristics of novel anode  $\text{Li}_4\text{Ti}_5\text{O}_{12}$ /polyacene materials for Li-ion secondary batteries. *Electrochim Acta* 53(12):4200–4204
- Bin Kim J, Kim DJ, Chung KY, Byun D, Cho BW (2010) Research on carbon-coated  $\text{Li}_4\text{Ti}_5\text{O}_{12}$  material for lithium ion batteries. *Physica Scripta* T139. doi:10.1088/0031-8949/2010/t139/014026
- Yuan T, Cai R, Shao ZP (2011) Different effect of the atmospheres on the phase formation and performance of  $\text{Li}_4\text{Ti}_5\text{O}_{12}$  prepared from ball-milling-assisted solid-phase reaction with pristine and carbon-precoated  $\text{TiO}_2$  as starting materials. *J Phys Chem C* 115(11):4943–4952
- Wang J, Liu XM, Yang H, Shen XD (2011) Characterization and electrochemical properties of carbon-coated  $\text{Li}_4\text{Ti}_5\text{O}_{12}$  prepared by a citric acid sol-gel method. *J Alloys Compd* 509(3):712–718
- Jung HG, Kim J, Seratosi B, Sun YK (2011) Micron-sized, carbon-coated  $\text{Li}_4\text{Ti}_5\text{O}_{12}$  as high power anode material for advanced lithium batteries. *J Power Sources* 196(18):7763–7766
- Li H, Shen L, Zhang X, Wang J, Nie P, Che Q, Ding B (2013) Nitrogen-doped carbon coated  $\text{Li}_4\text{Ti}_5\text{O}_{12}$  nanocomposite: superior anode materials for rechargeable lithium ion batteries. *J Power Sources* 221:122–127
- Zhang HQ, Deng QJ, Mou CX, Huang ZL, Wang Y, Zhou AJ, Li JZ (2013) Surface structure and high-rate performance of spinel  $\text{Li}_4\text{Ti}_5\text{O}_{12}$  coated with N-doped carbon as anode material for lithium-ion batteries. *J Power Sources* 239:538–545
- Zhao L, Hu YS, Li H, Wang Z, Chen LQ (2011) Porous  $\text{Li}_4\text{Ti}_5\text{O}_{12}$  coated with N-doped carbon from ionic liquids for Li-ion batteries. *Adv Mater* 23(11):1385–1388
- Wang YQ, Gu L, Guo YG, Li H, He XQ, Tsukimoto S, Ikuhara Y, Wan LJ (2012) Rutile- $\text{TiO}_2$  nanocoating for a high-rate  $\text{Li}_4\text{Ti}_5\text{O}_{12}$  anode of a lithium-ion battery. *J Am Chem Soc* 134(18):7874–7879
- Wang J, Zhao H, Yang Q, Wang C, Lv P, Xia Q (2012)  $\text{Li}_4\text{Ti}_5\text{O}_{12}\text{-TiO}_2$  composite anode materials for lithium-ion batteries. *J Power Sources* 222:196–201
- Rahman M, Wang JZ, Hassan MF, Wexler D, Liu HK (2011) Amorphous carbon coated high grain boundary density dual phase  $\text{Li}_4\text{Ti}_5\text{O}_{12}\text{-TiO}_2$ : a nanocomposite anode material for Li-ion batteries. *Adv Energy Mater* 1(2):212–220
- Kim JG, Shi D, Park MS, Jeong G, Heo YU, Seo M, Kim YJ, Kim JH, Dou SX (2013) Controlled Ag-driven superior rate-capability of  $\text{Li}_4\text{Ti}_5\text{O}_{12}$  anodes for lithium rechargeable batteries. *Nano Res* 6(5):365–372
- Zhu GN, Chen L, Wang YG, Wang CX, Che RC, Xia YY (2012) Binary  $\text{Li}_4\text{Ti}_5\text{O}_{12}\text{-Li}_2\text{Ti}_3\text{O}_7$  nanocomposite as an anode material for Li-ion batteries. *Adv Funct Mater* 23(5):640–647
- Matsui E, Abe Y, Senna M, Guerfi A, Zaghib K (2008) Solid-state synthesis of 70 nm  $\text{Li}_4\text{Ti}_5\text{O}_{12}$  particles by mechanically activating intermediates with amino acids. *J Am Ceram Soc* 91(5):1522–1527
- Yu L, Wu HB, Lou XWD (2013) Mesoporous  $\text{Li}_4\text{Ti}_5\text{O}_{12}$  hollow spheres with enhanced lithium storage capability. *Adv Mater* 25(16):2296–2300
- Liu J, Li X, Yang J, Geng D, Li Y, Wang D, Li R, Sun X, Cai M, Verbrugge MW (2012) Microwave-assisted hydrothermal synthesis of nanostructured spinel  $\text{Li}_4\text{Ti}_5\text{O}_{12}$  as anode materials for lithium ion batteries. *Electrochim Acta* 63:100–104
- Shen L, Uchaker E, Zhang X, Cao G (2012) Hydrogenated  $\text{Li}_4\text{Ti}_5\text{O}_{12}$  nanowire arrays for high rate lithium ion batteries. *Adv Mater* 24(48):6502–6506
- Pan H, Zhao L, Hu YS, Li H, Chen L (2012) Improved Li-storage performance of  $\text{Li}_4\text{Ti}_5\text{O}_{12}$  coated with C-N compounds derived from pyrolysis of urea through a low-temperature approach. *ChemSusChem* 5(3):526–529
- Mattia D, Rossi MP, Kim BM, Korneva G, Bau HH, Gogotsi Y (2006) Effect of graphitization on the wettability and electrical conductivity of CVD-carbon nanotubes and films. *J Phys Chem B* 110(20):9850–9855

33. Pierson HO (1993) Handbook of carbon, graphite, diamond, and fullerenes: properties, processing, and applications. Noyes Publications Park Ridge Chapter 3

34. Cheng L, Yan J, Zhu GN, Luo JY, Wang CX, Xia YY (2010) General synthesis of carbon-coated nanostructure  $\text{Li}_4\text{Ti}_5\text{O}_{12}$  as a high rate electrode material for Li-ion intercalation. *J Mater Chem* 20(3):595–602

35. Amine K, Belharouak I, Chen Z, Tran T, Yumoto H, Ota N, Myung ST, Sun YK (2010) Nanostructured anode material for high-power battery system in electric vehicles. *Adv Mater* 22(28):3052–3057

36. Jung HG, Myung ST, Yoon CS, Son SB, Oh KH, Amine K, Scrosati B, Sun YK (2011) Microscale spherical carbon-coated  $\text{Li}_4\text{Ti}_5\text{O}_{12}$  as ultra high power anode material for lithium batteries. *Energ Environ Sci* 4(4):1345–1351

37. Borgel V, Gershinsky G, Hu T, Theivanayagam MG, Aurbach D (2013)  $\text{LiMn}_{0.8}\text{Fe}_{0.2}\text{PO}_4/\text{Li}_4\text{Ti}_5\text{O}_{12}$ , a possible Li-ion battery system for load-leveling application. *J Electrochem Soc* 160(4):A650–A657

38. Ding Z, Zhao L, Suo L, Jiao Y, Meng S, Hu YS, Wang Z, Chen L (2011) Towards understanding the effects of carbon and nitrogen-doped carbon coating on the electrochemical performance of  $\text{Li}_4\text{Ti}_5\text{O}_{12}$  in lithium ion batteries: a combined experimental and theoretical study. *Phys Chem Chem Phys* 13(33):15127–15133

39. Franklin RE (1951) Crystallite growth in graphitizing and non-graphitizing carbons. *Proc Royal Soc Lond Ser A Math Phys Sci* 209(1097):196–218

40. Yuan T, Cai R, Gu P, Shao ZP (2010) Synthesis of lithium insertion material  $\text{Li}_4\text{Ti}_5\text{O}_{12}$  from rutile  $\text{TiO}_2$  via surface activation. *J Power Sources* 195(9):2883–2887

41. Zhou H, Zhu S, Hibino M, Honma I (2003) Electrochemical capacitance of self-ordered mesoporous carbon. *J Power Sources* 122(2): 219–223

42. Pan HL, Hu YS, Li H, Chen LQ (2011) Significant effect of electron transfer between current collector and active material on high rate performance of  $\text{Li}_4\text{Ti}_5\text{O}_{12}$ . *Chin Phys B* 20(11):118202-1–118202-4. doi:10.1088/1674-1056/20/11/118202

43. Yuan T, Wang K, Cai R, Ran R, Shao ZP (2009) Cellulose-assisted combustion synthesis of  $\text{Li}_4\text{Ti}_5\text{O}_{12}$  adopting anatase  $\text{TiO}_2$  solid as raw material with high electrochemical performance. *J Alloys Compd* 477(1–2):665–672

44. Li X, Qu M, Huai Y, Yu Z (2010) Preparation and electrochemical performance of  $\text{Li}_4\text{Ti}_5\text{O}_{12}$ /carbon/carbon nano-tubes for lithium ion battery. *Electrochim Acta* 55(8):2978–2982

45. Yuan T, Cai R, Wang K, Ran R, Liu SM, Shao ZP (2009) Combustion synthesis of high-performance  $\text{Li}_4\text{Ti}_5\text{O}_{12}$  for secondary Li-ion battery. *Ceram Int* 35(5):1757–1768

46. Lin ZJ, Hu XB, Huai YJ, Liu L, Deng ZH, Suo JS (2010) One-step synthesis of  $\text{Li}_4\text{Ti}_5\text{O}_{12}/\text{C}$  anode material with high performance for lithiumion batteries. *Solid State Ionics* 181(8–10):412–415